

Influence of irregularities in the rock underlayer on the stability of Xbloc^{Plus}

van den Berg, Ileen; Hofland, Bas; Reedijk, Bas

DOI

[10.1016/j.coastaleng.2020.103637](https://doi.org/10.1016/j.coastaleng.2020.103637)

Publication date

2020

Document Version

Accepted author manuscript

Published in

Coastal Engineering

Citation (APA)

van den Berg, I., Hofland, B., & Reedijk, B. (2020). Influence of irregularities in the rock underlayer on the stability of Xbloc^{Plus}. *Coastal Engineering*, 157, Article 103637. <https://doi.org/10.1016/j.coastaleng.2020.103637>

Important note

To cite this publication, please use the final published version (if applicable). Please check the document version above.

Copyright

Other than for strictly personal use, it is not permitted to download, forward or distribute the text or part of it, without the consent of the author(s) and/or copyright holder(s), unless the work is under an open content license such as Creative Commons.

Takedown policy

Please contact us and provide details if you believe this document breaches copyrights. We will remove access to the work immediately and investigate your claim.

Influence of irregularities in the rock underlayer on the stability of Xbloc^{Plus}

Ileen van den Berg^{a,c,*}, Bas Hofland^a, Bas Reedijk^b

^a*Department of Civil Engineering, Delft University of Technology, Stevinweg 1, 2628 CN, Delft, The Netherlands*

^b*Delta Marine Consultants, H.J. Nederhorststraat 1, 2800 AG, Gouda, The Netherlands*

^c*DPI — Dutch Process Innovators, Suikersilo Oost 33, 1165 MS, Halfweg, The Netherlands*

Abstract

Many rubble mound breakwaters are nowadays made with an armour layer consisting of single layer interlocking elements. The stability of these armour layers could well be influenced by the irregularity of the rock underlayer, as that influences the degree of interlocking. Especially for the new types of regularly placed armour, this might be an important factor for the stability. However, this aspect has not been studied widely yet. Therefore, this paper investigates the influence of irregularities in the underlayer on the stability of a type of single layer breakwater elements. Model tests have been conducted in which the irregularities in the underlayer were systematically varied. The irregularities in the underlayer and the orientations of breakwater elements were measured with 3D-scanning. The breakwater armour unit used in the tests is the Xbloc^{Plus}. A new failure mechanism, not previously observed for breakwater elements, was found to initiate damage. Causing the armour to be pushed outward by a combined effect of the weight of the upper armour

*Corresponding author; E-mail: i.vandenberg@dutchpi.com

and the excessive hydraulic pressure of the remaining water under the armour layer. Especially large-scale convex (i.e. protruding outwards) undulations in the cross-shore direction influenced the stability of the armour layer. This influence has been quantified.

Keywords: Breakwater, XblocPlus, armour layer stability, single-layer units, placement irregularity

1. Introduction

Background. Many rubble mound breakwaters are nowadays made with an armour layer consisting of concrete, single layer, interlocking elements. These armour layers obtain their stability not only from the weight of the single element on the slope, but also from interlocking and/or friction forces between the elements. Irregularities of the underlayer, typically made with randomly placed rocks of a smaller size, might influence the stability of the top layer of breakwater elements [Loman et al., 2012]. Still, to the authors knowledge, this aspect has hardly been studied. A logical explanation for the lack of in depth research in this area is the difficulty in finding a strong correlation between the underlayer configuration and the top layer stability. For randomly orientated elements not only the underlayer configuration influences the stability of the elements, but also the element orientation and placement densities [ten Oever et al., 2012]. Regularly placed elements such as the single layer cubes, Seabees and HARO's obtain their stability through lateral friction and are less sensitive for irregularities according to Van Gent and Luis [2013].

Recently however, new regularly placed elements such as the C-ROC [Per-

19 rin et al., 2017] and the Xbloc^{Plus}[Vos, 2017; Rada Mora, 2017] have been
20 developed to facilitate the placement procedure. The elements are placed
21 with both regular orientation and a regular placement grid, but obtain their
22 stability due to interlocking instead of lateral friction. The regular placement
23 reduces the fluctuations in element orientations and placement densities and
24 emphasizes the influence of the underlayer configuration on the interlocking
25 capacity and therefore the stability of the top layer. Especially since irregu-
26 larities in the underlayer are the cause of fluctuations in placement densities
27 and element orientations. At present, the tolerances for the underlayer used
28 during the execution of breakwaters with single layer elements are mainly
29 based on the experience in practice [Van der Zwicht, 2015] and are chosen
30 such that the placement of the breakwater elements is facilitated. A detailed
31 study on the influence on the stability lacks, such that the quantitative in-
32 fluence on the armour layer stability is unknown for any type of armour
33 unit.

34 *Aim.* It is suspected that irregularities in the underlayer are important for the
35 stability of regularly placed single layer elements. Hence this study focusses
36 on the influence of the irregularity of the underlayer on the stability of the
37 top layer. Possibly leading to guidelines for design criteria and construction
38 tolerances.

39 We want to know how the stability of the armour layer is influenced by
40 the size and direction of the distortions of the (otherwise straight) underlayer.
41 The main parameters that are of importance to the stability will be identified
42 and their influence will be quantified.

43 *Approach.* The element used during the research is the Xbloc^{Plus}, which is
 44 depicted in figure 1. Previous research on the element is used to provide
 45 insight in the mechanisms that are important for the stability of the ele-
 46 ment. The ongoing development programme of the new breakwater element
 47 Xbloc^{Plus}, provided an interesting opportunity for a study on the influence
 48 of the underlayer on their stability.

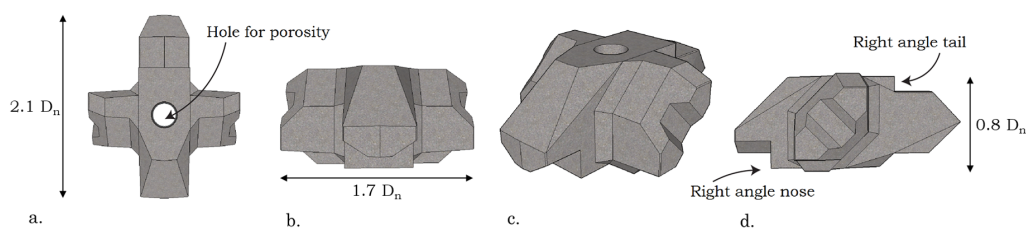


Figure 1: Shape of Xbloc^{Plus}, a) top view, b) front view, c) isometric view, d) side view

49 It is hypothesized that the stability of the elements decreases with de-
 50 creasing radius of the distortions of the (otherwise straight) underlayer.
 51 Moreover, it is thought that the direction of the irregularities is of impor-
 52 tance. These hypotheses were tested in 2D hydraulic model tests, where the
 53 irregularities were systematically varied, and the actual irregularities were
 54 measured in 3D. The results of the tests are used to validate the hypotheses
 55 and are further analysed to explain the observations. From the analysis fol-
 56 lows the conclusion on how the stability is influenced and which aspects are
 57 of importance to predict the level of stability.

58 *Outline.* The evaluation of previous research on the element is found in the
 59 next section. Based on this knowledge hypotheses are formed (section 3) on
 60 which the test program and model set-up are based (section 4). In section 5
 61 the processing of the 3D-data is explained, followed by the actual test results

62 in section 6. The analysis is explicated in section 7, resulting in the discussion
63 and conclusions.

64 **2. Previous research**

65 The Xbloc^{Plus} is an element that can be placed on straight, or in longitudi-
66 nal direction slightly curved breakwater or revetment sections. The elements,
67 shown in figure 1, are placed such that the same faces of the elements touch
68 the elements underneath. Resulting in a regular placement, with both a uni-
69 form grid and an uniform orientation. The blocks are typically placed on a
70 3:4 slope.

71 Multiple modifications have been applied during the development of the
72 Xbloc^{Plus}. The results of the research performed on these earlier versions have
73 gained insight in the influence of the modification and thereby on the aspects
74 that are of importance for the stability of the element. The first version of
75 the Xbloc^{Plus} was without the hole in the middle of the element and with
76 chamfers instead of right angles at the nose and tail of the element (figure 1).
77 The mechanism that governed the stability of this version was identified by
78 Vos [2017]. The conclusion of the research was that failure occurred due to
79 rotation of an element due to the drag during up-rush, after which extraction
80 occurred as a result of uplift pressure on the armour layer (figure 2).

81 For the second version the hole was added to enlarge the porosity and
82 reduce the uplift pressure. An increase in stability proved that the excessive
83 uplift pressure is indeed a dominant factor for the stability. To improve
84 the stability further, the interlocking capacity was enlarged by replacing the
85 chamfers by right angles (figure 1). This improved the stability to such extent

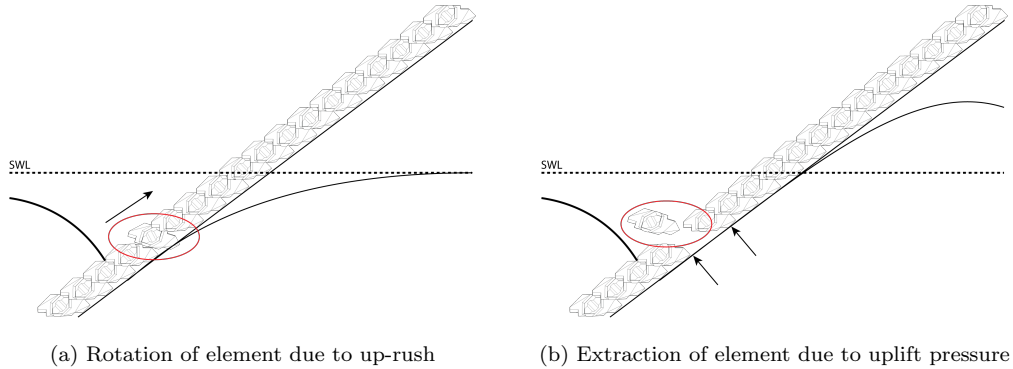


Figure 2: Failure mechanism for the first version of Xbloc^{Plus}[Vos, 2017]

86 that failure no longer occurred at the tested scale and available wave facility.
 87 The maximum achieved stability number $N_s = H_s / \Delta D_n$ was 4.0, where H_s is
 88 the incoming significant wave height, Δ the submerged dimensionless density,
 89 and D_n the nominal diameter of the element [Jacobs, 2017]. So the limit
 90 value of the stability number for this breakwater element was concluded to
 91 be higher than 4.0. Although it must be marked that these tests were done
 92 with a fixed toe and no safety margins have been included. As the tests were
 93 done with a straight, well-placed slope, the question arose how susceptible
 94 the element was to irregularities of the underlayer.

95 Several damage mechanisms have been identified for single layer break-
 96 water elements [Garcia et al., 2013]. Rocking is not very important for the
 97 Xbloc^{Plus} as all elements are embedded. Since the replacement of the cham-
 98 fers for the right angles, this phenomenon has only been observed directly
 99 before extraction. Also a displacement of the toe structure was seen to loosen
 100 the packing of several single layer armour types, which can lead to extrac-
 101 tion of elements and failure of the armour layer [Hofland and van Gent, 2016].
 102 This potential cause of damage was not tested yet for the Xbloc^{Plus}.

103 It has been discussed before that the underlayer can influence the top layer
104 stability for single layer (cubes) [Loman et al., 2012]. For the C-Roc block
105 only the grading width of the underlayer was varied somewhat ($M_{85}/M_{15} =$
106 1.8 to 4.2, where M_{85} and M_{15} are the 85% and 15% percentiles of the
107 grading curve of the underlayer rock). It was reported that this change of
108 the underlayer did not noticeably change the stability of the top layer [Perrin
109 et al., 2017].

110 Detailed 3D measurements of the toplayer surface of a Cubipod armour
111 layer have been performed by Pardo et al. [2013]. The goal of this research
112 was to measure the amount of randomness, which needed to be maximized
113 for this particular breakwater element type, while the current research is
114 focussed on small deviations from a regular pattern.

115 **3. Hypotheses**

116 The improved stability due to the introduction of the right angles at the
117 nose and tail of the Xbloc^{Plus} elements indicates the influence of interlocking
118 on the level of stability. Therefore, it was expected that the amount of
119 interlocking would be a key factor for the influence of irregularities in the
120 underlayer on the stability of the Xbloc^{Plus}. Hence, theoretical relative angles
121 between elements were determined for which the elements were no longer
122 sufficiently interlocked and a significant drop of stability was expected. For
123 the cross shore angles, the interlocking is lost when the right angle below the
124 nose of the upper unit no longer hooks behind the lower unit. Long shore
125 the interlocking was lost when the 'wings' of the elements were no longer
126 supported by the two lower elements. The angles for which interlocking was

127 lost were determined for each combination of shape (convex and concave) and
 128 direction (cross shore and long shore). These critical angles are indicated in
 129 Figure 3. An overview of the expected critical relative angles is given in
 130 Table 1.

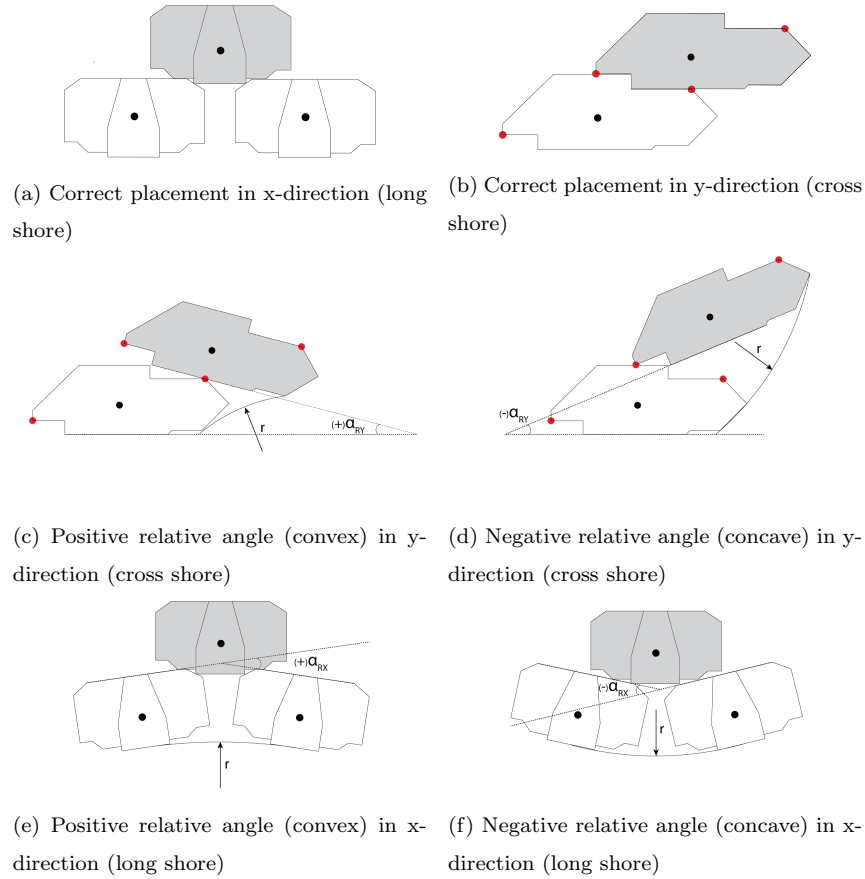


Figure 3: Definitions of critical relative angles and radii, pertaining to upper (grey) elements in the figures

131 The shapes in long shore direction were expected to be the least critical,
 132 since these shapes only cause a distortion of the grid and no direct loss of
 133 interlocking. The initial rotation caused by a convex shape in cross shore

Direction	Shape configuration	Relative angle	Critical radius
Cross shore	Convex	(+) 23°	3.0 D _n
	Concave	(-) 15°	4.4 D _n
Long shore	Convex	(+) 38°	3.0 D _n
	Concave	(-) 18°	6.0 D _n

Table 1: Expected critical values

134 direction is similar to the rotation in the first stage leading to failure (figure
135 2a). Therefore, this configuration was expected to be critical. For a regular
136 Xbloc, a convex (protruding), cross shore undulation was also seen to be the
137 most influencing type of irregularity [Brouwer, 2013].

138 Next, these critical angles have been translated to the radius of curvature
139 of the underlayer, for which these angles are expected to occur (also indicated
140 in figure 3). It is hypothesized that this radius of curvature of the underlayer
141 is of influence on the stability of the layer, and that a strong decrease of
142 stability occurs if the occurring curvature becomes smaller than these critical
143 curvatures.

144 The previously determined hypotheses were also expected to be valid for
145 more realistic configurations. Relevant realistic configurations are micro-
146 irregularities with length scales of several diameters of the rock of the under-
147 layer (see figure 4a) and S-profiles [Van der Meer, 1988] that can be present
148 in the underlayer due to small storms during construction (figure 4b).

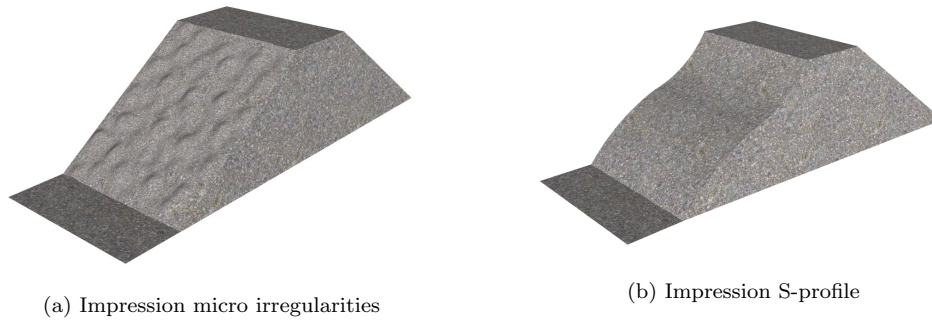


Figure 4: More realistic irregularities

149 **4. Model set-up**

150 The influence of irregularities on the stability of the Xbloc^{Plus} is deter-
 151 mined by performing physical model tests. The cross section of the tested
 152 structure is depicted in figure 5.

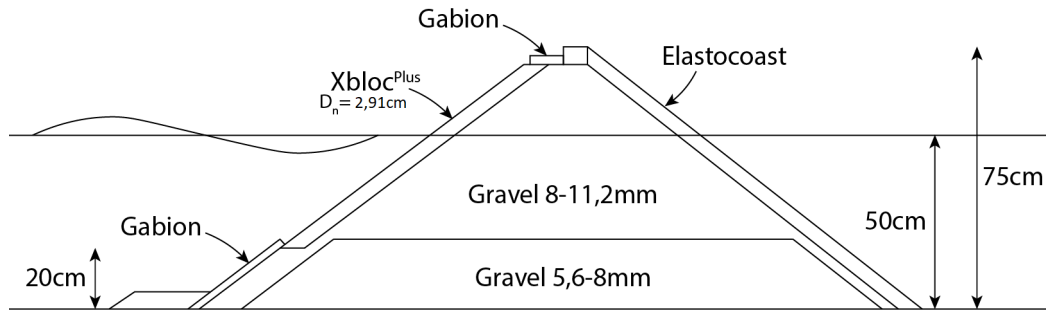


Figure 5: Cross section of the model structure geometry

153 The tests are performed with a slope of 3:4 because a steep slope is
 154 expected to be more conservative with regards to the stability [Angremond
 155 et al., 2008]. The freeboard was chosen to be 2.5 times the $H_{s,design}$. $H_{s,design}$ is
 156 the design wave height chosen by block developers Delta Marine Consultants
 157 as the wave height that leads to a conservatively stable stability number of
 158 2.5. The maximum tested H_s is 1.5 times this $H_{s,design}$. Resulting in relatively

159 few waves reaching the crest of the structure. This was chosen such because
160 the stability of the crest is not an objective of this research.

161 The model elements had a D_n of 2.91cm, a relative density of 1.36 g/l, a
162 width of 4.88cm, a height of 2.44cm, and a length of 6.19cm. The Reynolds
163 number ($\sqrt{gH_{s,\text{design}}}D_n/\nu$) is below $3 \cdot 10^4$ and therefore underneath the limit
164 where non-developed turbulent flow inside the porous medium starts to in-
165 fluence the stability of the top layer [Dai and Kamel, 1969].

166 The guideline of DMC for the W_{50} ratio between the underlayer and
167 breakwater elements is between 1/10 and 1/20. The underlayer and core are
168 of the same grading to prevent deviations in thickness of the underlayer, that
169 could influence the results by causing a varying porosity. The combined core
170 and underlayer is chosen to be of the standard grading of 8-11.2mm, which
171 gives a W_{50} of $\approx 1/20$.

172 The crest and toe are outside the scope of this study and built with a
173 higher stability than expected in reality to prevent failure at these locations.
174 The target fictitious deep water wave steepness was $s_{\text{op}}=0.04$. Which is a
175 commonly used wave steepness to represent wind waves in design storms
176 [Angremond et al., 2008].

177 The model tests are conducted in the wave flume of Delta Marine Con-
178 sultants in Utrecht, the Netherlands. This flume is 60cm wide, 100cm high
179 and has a length of 25m. All tests are performed with a constant water
180 depth of 50cm and without a foreshore to prevent breaking of the waves be-
181 fore the structure is reached. The maximum applied wave height is $H_s =$
182 16cm. The waves are irregular based on a JONSWAP-spectrum with $\gamma=3.3$
183 and each test consists out of 1000 waves. The flume has a piston-type wave

184 board with an Active Reflection Compensation system, which damps out the
 185 reflected waves.

186 *Test program.* The total test program is subdivided into seven test-sections,
 187 each test-section is testing a specific type of irregularity and consists out of
 188 various test series. All test series are conducted with different sizes and/or
 189 locations of the type of irregularity. In total 26 test series have been per-
 190 formed, with a total of 177 test runs. Each test series consisted of two to six
 191 separate test runs with stepwise increasing wave height by 20% or 10% until
 192 damage occurred, or until the limit of the wavemaker was reached. Some
 193 representative conditions of the various test runs are given in table 2

Test run	H_s	T_p	N_s	$\frac{H_{0.1\%}}{H_s}$
1	0.0639	0.99	1.6	1.94
2	0.0834	1.14	2.1	1.93
3	0.102	1.29	2.6	1.85
4	0.122	1.40	3.1	1.77
5	0.132	1.42	3.3	1.62
6	0.138	1.55	3.5	1.73
7	0.146	1.58	3.7	1.56
8	0.154	1.57	3.9	1.52

Table 2: Representative test conditions per run

194 Out of the 26 test series, only 11 series resulted in failure. This limits
 195 the certainty of when exactly failure will occur. However, the tests without
 196 failure do yield a conservative lower bound for the critical damage number.

197 The test program is divided in three separate parts. Part I consists of test-
 198 section 1, and has the goal to determine the stability without any intentional
 199 irregularities. It is the reference case to which the other test-sections can be
 200 compared to and the effect of the irregularities is determined with. Part II
 201 covers test-sections 2 up to 5, which are the series with macro irregularities
 202 in different directions and shapes. The goal of this part of the test program
 203 is to either validate or disprove the stated hypotheses. In part III, the final
 204 part of the test program, more realistic configurations are tested. Part III
 205 comprises test-sections 6 and 7.

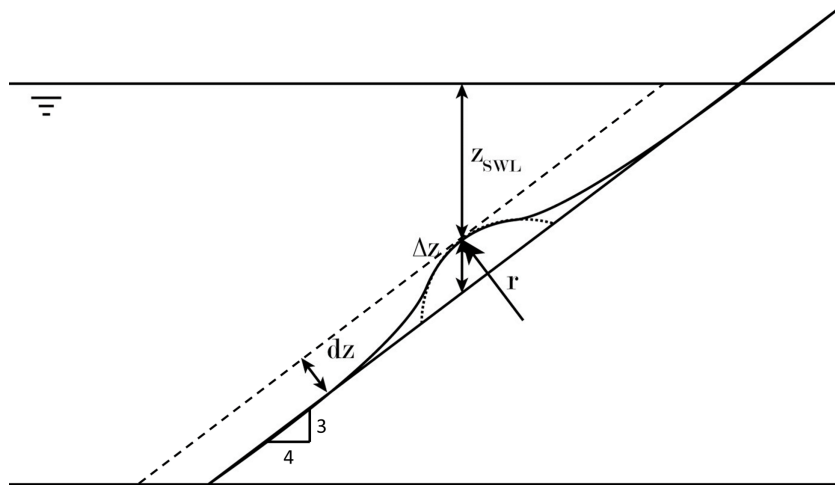


Figure 6: Aspects relevant for target size and location

206 For part II, each series within the test-section has a different size and/or
 207 location of the specific type of irregularity. An overview of all the different
 208 series and their specific irregularities is given in Table 3. The target values for
 209 the size and location of the irregularities is also given in this table. The target
 210 value for the radius of the irregularity is given relative to the hypothetical
 211 critical radius. The maximum vertical deviation from the design profile is

212 given as Δz . The location of the irregularity along the profile is given relative
 213 to the Still Water Level, indicated by z_{SWL} . Both values are given relative to
 214 the breakwater element size (D_n). Figure 6 shows the geometrical notations.

Part	Section	Irregularity type		Series	Target size and location			# Runs	$N_{s,max}$
		Direction	Shape		$\frac{r}{r_{hyp}}$	$\frac{dz}{D_n}$	$\frac{z_{SWL}}{D_n}$		
I	1	N.a.	Straight slope	1	n.a.	n.a.	n.a.	8	> 3.9
II	2	Cross shore	Convex	1	1.0	1.0	-3.4	5	3.3
				2	1.2	1.0	-3.4	8	> 3.9
				3	0.8	1.0	-3.4	2	2.0
				4	1.0	0.8	-3.4	7	3.8
				5	1.0	1.0	0.0	8	> 4.1
	3	Cross shore	Concave	1	1.0	1.0	0.0	8	> 4.2
				2	0.8	1.0	0.0	8	> 3.9
				3	1.0	1.0	-3.4	7	3.7
				4	1.0	1.0	-1.7	8	> 3.9
	4	Long shore	Convex	1	1.0	1.0	n.a.	8	> 3.9
				2	1.2	1.0	n.a.	8	> 4.0
	5	Long shore	Concave	1	1.0	1.0	n.a.	8	> 3.9
				2	1.0	1.0	n.a.	8	> 4.2
				3	0.8	1.0	n.a.	8	> 4.0

Table 3: Overview test configurations, part I and II

215 In part III the irregularities are present over the full length and width of
 216 the test area. In test-section 6 the irregularities are randomly applied, there-
 217 fore the sizes are not specific but an estimated value. The values are given in
 218 table 4. The S-profile configurations in test-section 7, are made by applying
 219 a certain $H_s/\Delta D_n$ to the underlayer. D_n is the nominal model element di-
 220 ameter of the side of the volume equivalent cube, which is approximately 20
 221 times the D_{n50} of the underlayer. Multiple tests have been done with differ-
 222 ent wave heights and durations of application, an overview of the differences
 223 is given in table 5. If another size of underlayer is used than was used for the
 224 present tests, or if different wave heights occur during construction, different
 225 S-profiles can occur in the under layers. Hence the size of the irregularity

226 (dz) is used as the parameter to quantify the influence of the irregularity on
 227 the block stability.

Part	Section	Irregularity type		Series	Target size		# Runs	$N_{s,max}$
		Direction	Shape		Below SWL $\left[\frac{dz}{D_n}\right]$	Above SWL $\left[\frac{dz}{D_n}\right]$		
III	6	All	Micro irregularities (figure 4a)	1	1.0	1.0	8	> 4.0
				2	1.1	1.1	8	> 3.9
				3	1.2	1.2	8	3.7
				4	1.2	1.0	6	3.1
				5	0.8	0.8	8	> 3.9

Table 4: Overview test configurations, part III test-section 6

Part	Section	Irregularity type		Series	Applied waves		# Runs	$N_{s,max}$
		Direction	Shape		$\frac{H_s}{\Delta D_n}$	Duration [min]		
III	7	Cross shore	S-profiles (figure 4b)	1	1.5	≈ 7	3	2.6
				2	1.5	≈ 2	8	> 3.9
				3	1.5	≈ 5	3	2.5
				4	1.0	≈ 10	6	3.5
				5	1.3	≈ 10	6	3.7
				6	1.4	≈ 10	4	3.1

Table 5: Overview of test configurations, part III test-section 7

228 The number of series within each test-section was not known beforehand
 229 and is based on the output of the previous tests. The goal is to obtain the
 230 stability parameter for different sizes of the irregularities, so a critical value
 231 can be determined. If failure occurs during an early run, the next test is
 232 performed with an irregularity of a smaller size. Vice versa, the irregularity
 233 is increased when failure occurs at high wave heights or not at all. The
 234 irregularity is not increased beyond the boundaries of what would be realistic
 235 in practice. In that case the test program is continued with the next test-
 236 section.

237 5. Digital Elevation Model processing

238 The angle of the elements relative to its neighbouring elements is consid-
239 ered to be the aspect of interest. Therefore, the orientations of all elements
240 in the test section needed to be measured. The orientations were obtained
241 from a Digital Elevation Model (DEM). This DEM was obtained from a
242 point cloud that was created with Autodesk ReCap, based on about 50 pho-
243 tos made by a Huawei P9lite 13 Mpix mobile phone camera. The conversion
244 from 3D-point clouds to DEM and subsequent processing was done in Python.

245 Each test configuration was measured both at the beginning of the test
246 series and after the last test was performed. At these moments the configura-
247 tion of both the underlayer and the armour layer were measured, unless the
248 damage after the test runs was too severe for the model to be meaningful. At
249 the beginning of each test two sets of 40-60 photos were made, from which
250 three models were created. One model of each photo set and one model of (a
251 random selection of) the combined photo sets. The multiple DEM's enable
252 us to estimate the accuracy of the recordings, and averaging over the three
253 models reduces the random errors. At the end of the test series only one set
254 of photos was taken.

255 The ReCap program calculates a point cloud from the set of photos,
256 which is shown in figure 7. The point clouds have 41000 to 45000 points in
257 the region of interest. From the point cloud the points in the test section
258 are extracted. For each point the x,y,z-coordinates and the RGB color values
259 are determined. The z-axis is defined upward from the bottom of the flume,
260 the y-axis in the length of the flume and the x-axis over the width of the
261 flume with its origin at the left side of the flume (facing the slope). All the

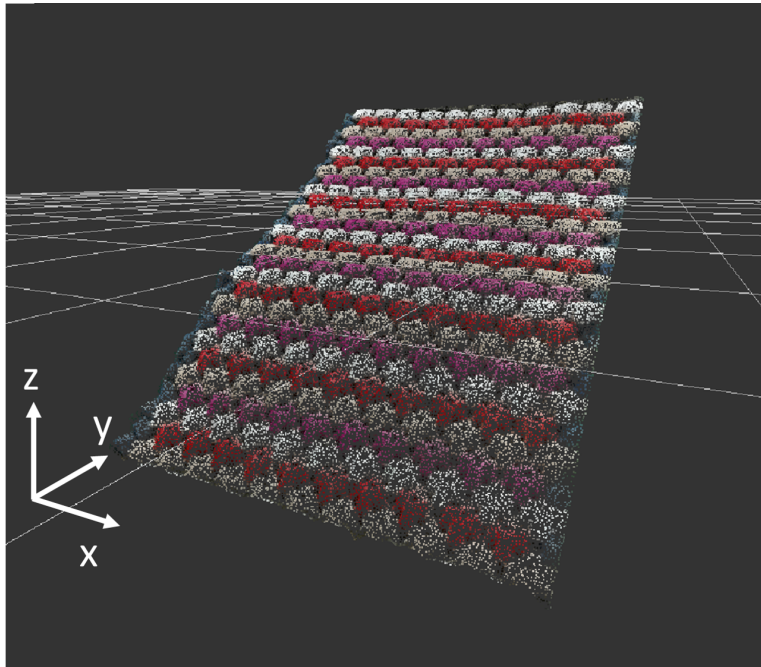


Figure 7: Example ReCap point cloud

262 models are fixed in the same axial system by using four fixed targets. Two
263 on each side of the wave flume, one at the level of the crest and one just
264 above the first row of breakwater elements. Each target of each model is
265 selected manually in ReCap. To reduce errors in the target registration the
266 zoom function of the program was used and each target has been selected on
267 at least eight pictures.

268 The point cloud is loaded into Python and reinterpolated onto a regular
269 x,y-grid for further processing, resulting in a DEM with a grid spacing of
270 0.00025m.

271 Next, the separate elements need to be identified. With the x,y-coordinates
272 and the colour values a top view is compiled from which the element locations

273 are determined with the MatchTemplate routine by OpenCV [Docs.opencv.org].
 274 The element locations are checked visually during processing, in both the
 275 compiled top view and the plot of the z-coordinates relative to the straight
 276 target profile (without irregularity). Figure 8 shows an example of these top
 277 views of the DEM of a test series 1 from section 2 (convex in cross shore
 278 direction) with indications of the automatically identified locations of the
 279 elements.

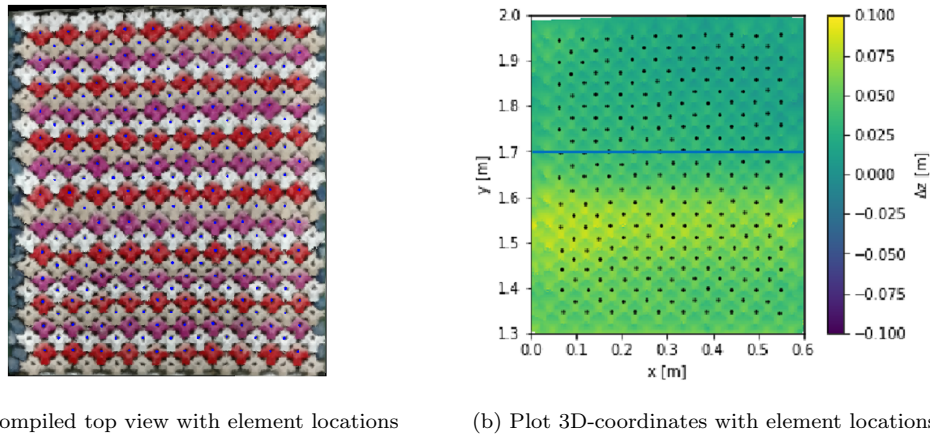


Figure 8: Check of element locations of section 2 (convex in cross section) test series 1

280 The orientation of the top of the element is determined in x and y direc-
 281 tion at the element locations and recalculated into angles. To prevent small
 282 measurement errors from affecting the result, the slope is averaged over a
 283 square area of 25mm^2 in the x,y-plane, around the centre of mass of the ele-
 284 ment. This area was chosen as a compromise between cancelling out model
 285 noise and preventing errors due to inaccuracy of the element locations.

286 The corresponding orientation of the underlayer at the element locations
 287 are measured as well. This is measured at the location where the tail of

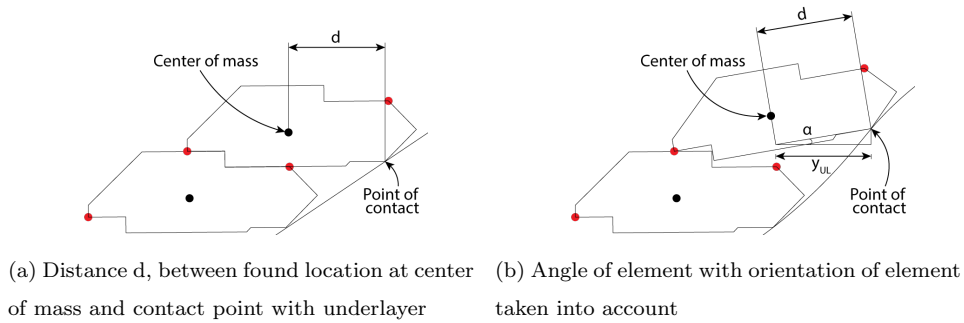


Figure 9: Calculating corresponding location underlayer

288 the breakwater element contacts the underlayer, as is depicted in figure 9.
 289 To prevent single grains from affecting the slope of the profile, the DEM is
 290 smoothed with a Gaussian filter with a standard deviation equal to the D_{n50}
 291 of the underlayer. The result of smoothing is depicted in figure10, in which
 292 indeed it can be seen that the individual grains are smoothed out while the
 293 larger profile deviations are maintained.

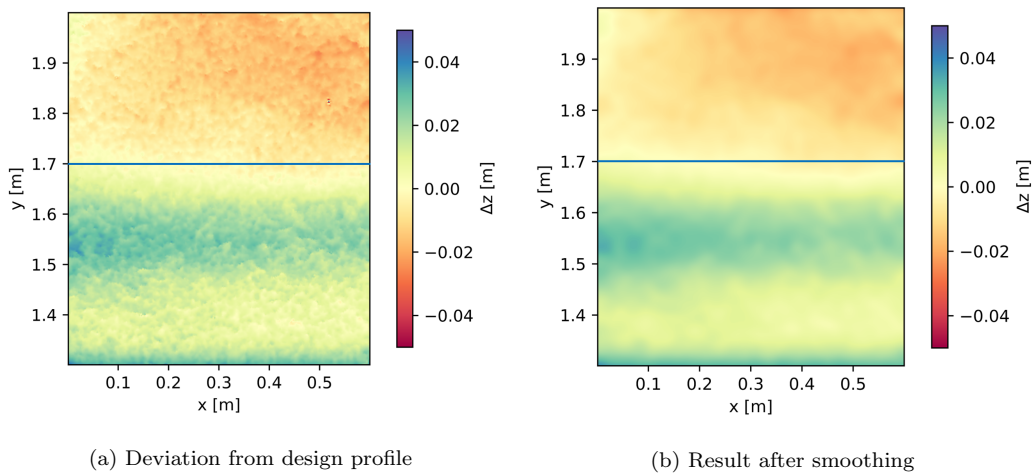


Figure 10: Effect from electronic smoothing of underlayer test series 1 section 2 (convex in cross section)

294 Further reduction of measurement errors is accomplished by averaging
 295 the angles of each location over the three models that have been made at the
 296 same moment. After averaging, the relative angles are calculated.

297 In y-direction the relative angle (α_{RY}) is calculated as the angle of the
 298 element minus the average angle of the two supporting elements underneath.
 299 In x-direction the relative angle (α_{RX}) depends on the two elements under-
 300 neath, it is calculated as the angle between the two elements. The exact
 301 definitions of the positive and negative relative angles for both directions is
 302 visualised in figure 3.

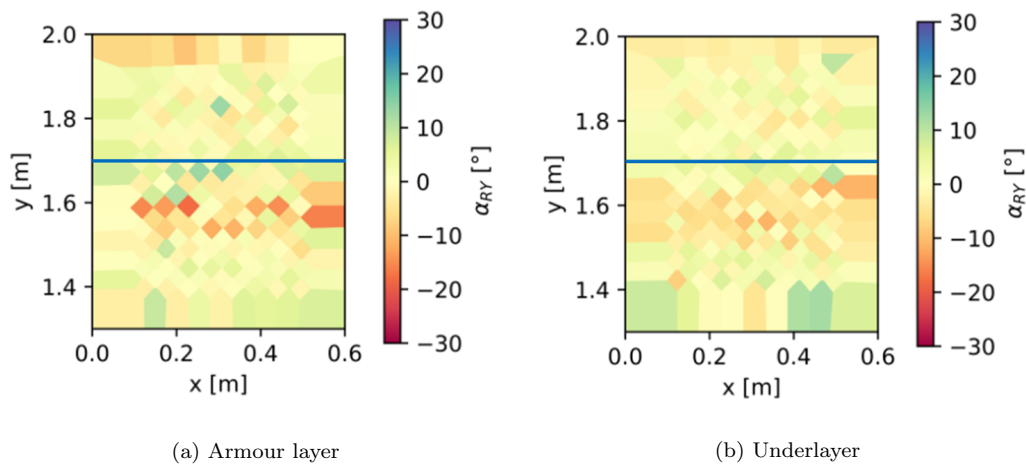


Figure 11: Calculated relative angles of section 2 (convex in cross section) test series 1

303 The results of the relative angles for the same case are visualised at the
 304 locations of the elements as in figure 11. These fields with relative angles
 305 have been created for all test series.

306 For all test series, the relative angles are extracted for the breakwater
 307 element where failure occurred and related to the N_s for which the failure
 308 occurred. If no failure occurred the maximum measured values of α_R and

309 N_s are taken. This constitutes the final information that is used for further
310 analysis. The same is done with the relative angle of the corresponding
311 underlayer.

312 The three ReCap models made at the same moment are compared to
313 indicate the accuracy of the data. For each test series the three models have
314 been compared to the average of the three models combined.

315 The average standard deviation of each point over the three models is less
316 than 1mm. The maximum deviation between the models is 5mm. This maximum
317 deviation however, occurs at the transition between elements. At the
318 top of the element, where the data for the element orientation is extracted,
319 the maximum deviation is 3mm. For the underlayer there are exceptions
320 where the deviation is 5mm, most models have a maximum deviation of
321 3mm. The calculated angles have an average standard deviation of 2.2° for
322 the armour layer and 0.4° for the underlayer in both x- and y-direction. The
323 errors are expected to be random and to be further reduced by averaging
324 over the three models.

325 **6. Test results**

326 All tests were executed according to plan. In many test series, no extrac-
327 tion of units could be obtained for the top layer with the capabilities of the
328 wave facility. In these series it could only be concluded that $H_s/\Delta D_n > 4$.

329 The hypothesis are based on the assumption that the orientation of the
330 breakwater elements is influenced by the condition of the underlayer. In
331 Figure 12 an example is shown of the S-profiles where it can be seen that the
332 measured angles of the underlayer indeed correspond to the measured angles

333 of the element orientations.

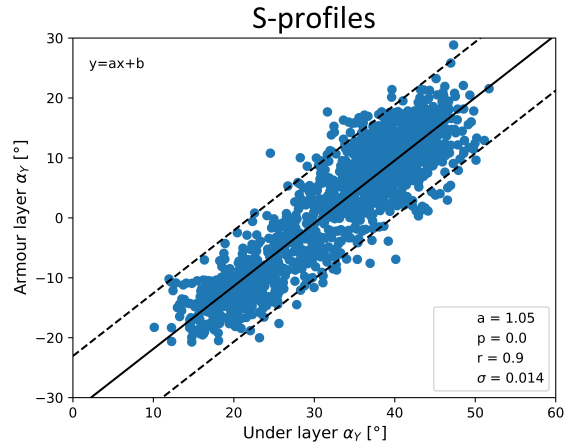
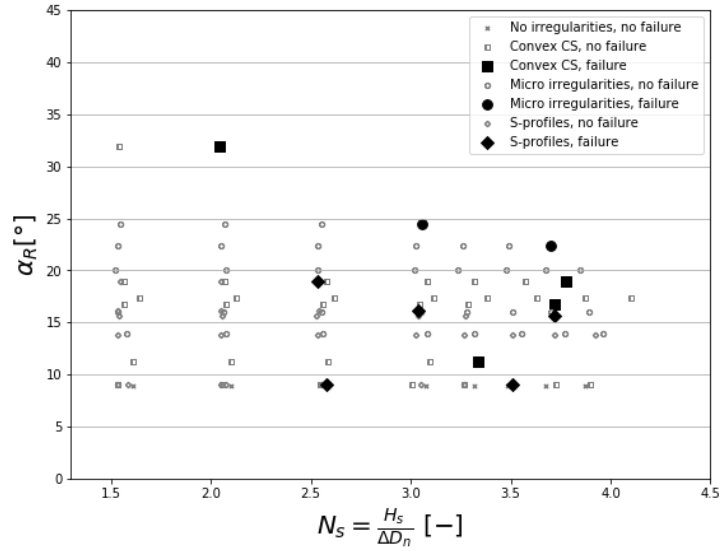


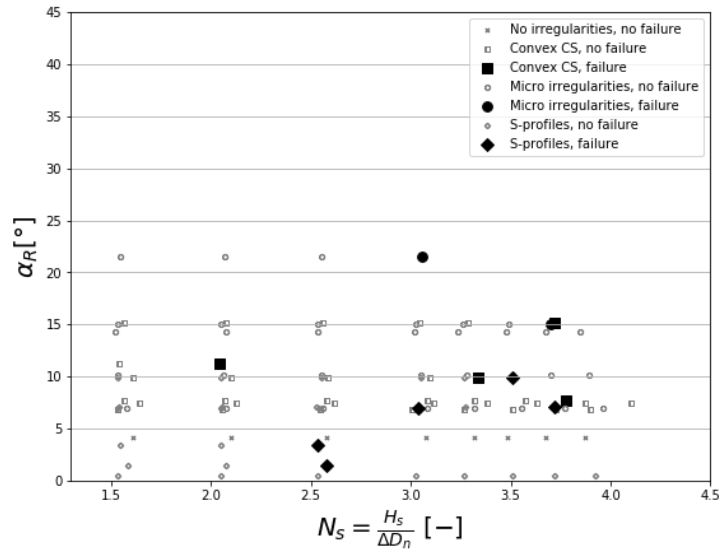
Figure 12: Correlation between angles measured for S-profile tests in underlayer and armour layer

334 The convex shape in cross shore direction resulted to be, as expected in
335 the hypotheses, the most critical configuration. This was the only shape for
336 which failure occurred during the test program. For the other shapes and
337 directions no failure occurred and these tests are thus not further discussed
338 in this paper. Also in Part III of the test program, failure occurred only at
339 the areas with a convex shape in cross shore direction. The measured relative
340 angle of the failed elements are related to the N_s for which failure occurred.
341 The preceding tests without failure are given for reference in Figure 13.

342 For both the armour and underlayer a large spreading can be seen in the
343 results and no clear dependency between α_{RY} and $H_s/\Delta D_n$ can be derived.
344 The measured relative angles of the underlayer are smaller than the resulting
345 angles of the elements. This is expected to be an effect of the smoothing
346 applied to the measured underlayer.



(a) Armour layer



(b) Corresponding underlayer

Figure 13: Correlation N_s and α_R ; black markers indicate failure

347 It is observed during the tests and from the test results that test series
 348 with approximately the same relative angles had an earlier failure when the

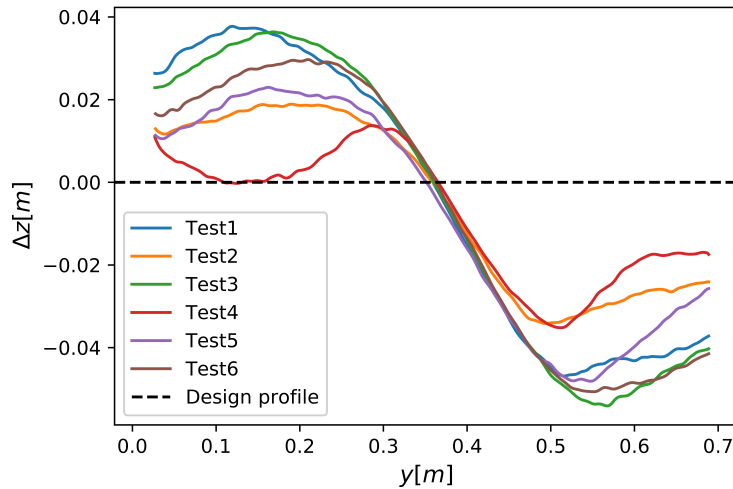


Figure 14: Measured deviations of the underlayer from the design profile of the S-profiles in test section 7

349 deviation from the design profile was larger. An example of the differences
 350 in deviation from the design profile is given in Figure 14.

351 Additionally, it was observed during the tests that, especially during sud-
 352 den failure, the lower part of the slope moved away from the slope and the
 353 upper part moved downward. This was also seen in the measurements of the
 354 vertical differences between the start and end of the test series, as well for
 355 test series that failed as for test series where no failure occurred (Figure 15).

356 7. Analysis

357 The large spreading in the test results indicated that the relative angles
 358 between neighbouring elements are not the only factor of influence. It was
 359 seen that configurations with approximately the same relative angle (α_R) but
 360 a larger deviation from the design profile resulted in earlier failure. Which led

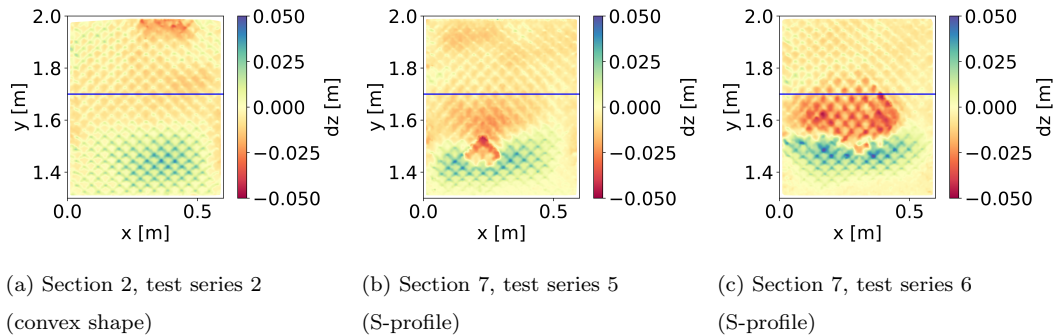


Figure 15: Measured difference in vertical elevation of the armour layer between start and end of test series

361 to the expectation that the deviation from the design profile influences the
 362 stability as well. The results showed that more specifically the steepness of
 363 the lower part of the convex shape is a good indicator of the influence on the
 364 stability. For many types of elements, a steeper slope decreases the strength
 365 of the top layer [Hudson, 1959]. Subsequently, this steepness is influenced by
 366 both the absolute deviation from the design profile and the length over which
 367 the deviation occurs. This is expressed in the additional parameter β , which
 368 is the average additional angle resulting from the deviation from the design
 369 profile. Measured as the angle resulting from the length (L1) between the
 370 lower edge of the protrusion ($\Delta z' \approx 0$) and the top of the convex shape and
 371 the difference at the top of the convex shape between the measured profile
 372 and the design profile, as is visualised in Figure 16.

373 Parameter β is considered to be zero for the (small scale) micro irregular-
 374 ities. With this assumption taken into account, empirical results showed that
 375 the summation of α_R and β results in a significant reduction of the spreading
 376 in the results as can be seen in Figure 17.

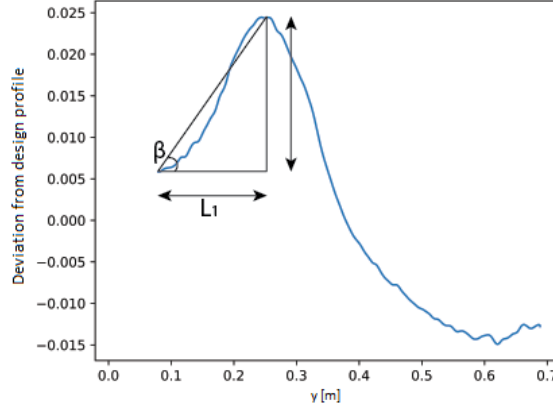


Figure 16: Visualisation β

377 The resulting trend line of the armour layer is given by equation 1. The
 378 trend line of the corresponding underlayer is given by equation 2.

$$\text{Armour layer} : N_s = -0.1(\alpha_R + \beta) + 5.7 \quad (1)$$

$$\text{Underlayer} : N_s = -0.3(\alpha_R + \beta) + 8.2 \quad (2)$$

379 The influence of β on the stability of the profile can be explained on the
 380 basis of an extremely simplified model. The model is based on the S-profiles
 381 since the influence of β was seen best during testing in these profiles.

382 In the model the elements above and underneath the top of the convex
 383 shape are considered to be two rigid bodies. Thus assuming that the elements
 384 inside the rigid bodies are fully interlocked. The lower rigid body is fixed
 385 with a hinge at the lower edge of the protrusion and linked with a hinge to the
 386 upper rigid body. The upper rigid body is considered to be connected to the
 387 design profile with a roller bearing by means of a hinge. The schematisation

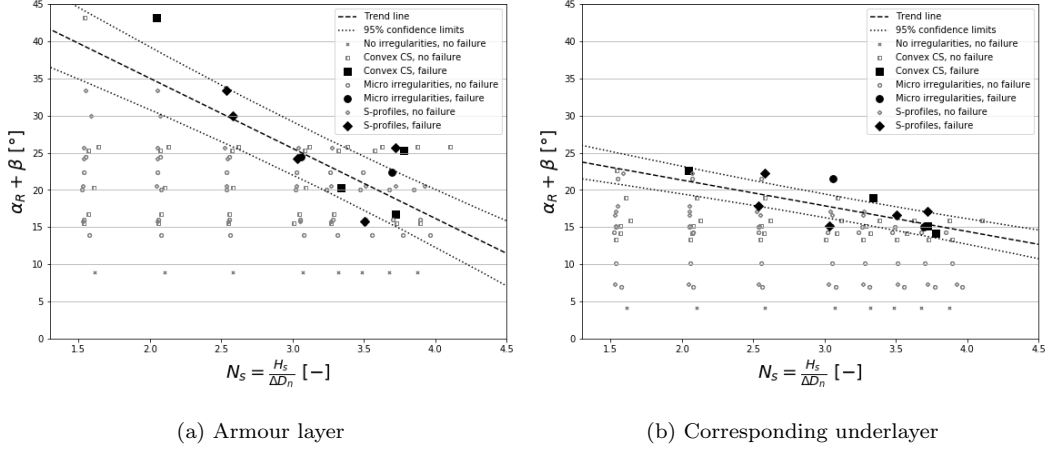


Figure 17: Correlation N_s and $\alpha_R + \beta$

388 and visualisation of the simplified model is given in Figure 18.

389 The up- and down-rush of the waves takes place along the upper rigid
 390 body. The most critical moment is considered to be during maximum run-
 391 down. Assumed is that the gravity force of the upper rigid body is then fully
 392 counteracted by the pressure force underneath the body. The only modelled
 393 force on this body is the effective drag force ($F_{d_{\text{eff}}}$). The effective drag force
 394 is the drag force, complemented by the weight of the elements above the
 395 convex section, minus the friction of the underlayer. This force causes a
 396 rotation of both the rigid bodies resulting in an enlarged relative angle. The
 397 only modelled force on the lower rigid body is the gravity force. This is the
 398 resistive force against the movement of the rigid bodies.

399 The angles α_R and β are dependent of each other, this relation can be
 400 described by the following formula.

$$\alpha_R \approx \beta \left(1 + \frac{L_1}{L_2} \right) \quad (3)$$

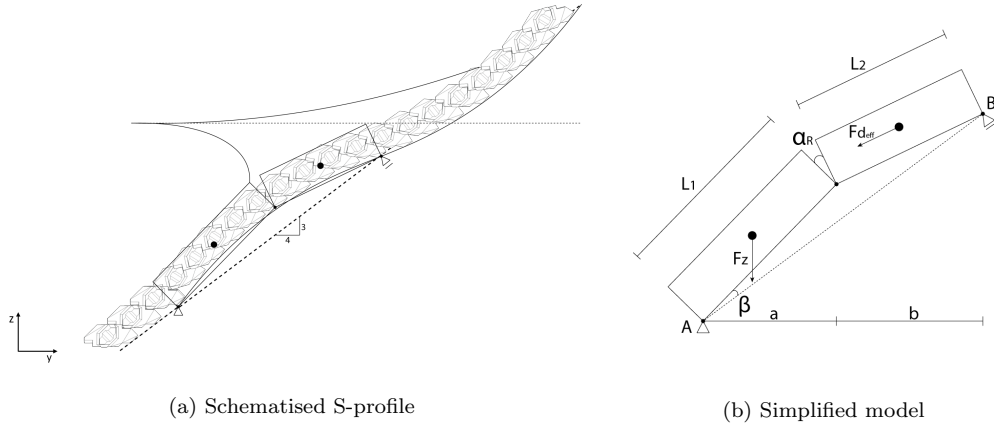


Figure 18: Schematisation of S-profile into simplified model

401 An increase of β results a reduction of the leverage arm of the resistive
 402 force around point A. Thereby reducing the resistance against rotation of the
 403 rigid bodies. An increase of α_R enlarges the leverage arm of the acting force
 404 ($F_{d_{eff}}$) around point A and induces the rotation of the rigid bodies. Thereby
 405 explaining the influence of these parameters on the stability. If the resistive
 406 moment is smaller than the acting moment, the rigid bodies are lifted away
 407 from the underlayer. Resulting in an enlargement of the convex shape and
 408 α_R , ultimately causing failure.

409 The movements indicated by the simplified model, have been measured
 410 in the tests. For tests both with and without element extraction, as can
 411 be seen in Figure 15. The movements seen in the measurements however
 412 slightly deviate from the movements indicated by the simplified model. Since
 413 the upper rigid body fully subsides in the simplified model instead of only
 414 partially, as can be seen in the measurements. This difference could be due
 415 to the fault that the model does not take the movements of the underlayer
 416 into account. When the lower elements move away from the underlayer, the

417 underlayer is no longer stable and the grains will move downward. Which
418 causes the upper rigid body to subside.

419 The analysis indicates that the relative angle between the elements at
420 the top of the convex shape (α_R) determines whether it is possible for the
421 element to be extracted from the profile. The steepness (β) of the slope
422 downward from this point however, can cause an enlargement of (α_R) and
423 therefore influences the level of stability as well.

424 8. Discussion

425 The wavemaker is piston-type, a rule-of-thumb for the maximum gener-
426 ated waves in a given water depth is around half the water depth, i.e. 0.25m.
427 The maximum applied wave height is $H_s = 0.16\text{m}$, assuming Rayleigh dis-
428 tribution and 1000 waves, the maximum wave height should be around 0.31
429 m. This means that the maximum waves in the extreme sea state will break
430 near the wavemaker, so the wave height distribution is trimmed in the upper
431 tail. This is one of the possible reasons the maximum waves in the sea states
432 were not achieved (see table 2) and as a consequence, initiation of damage
433 was not reached in most of the test series carried out.

434 The radii of the hypothetical critical irregularities in cross shore direc-
435 tion were much smaller than the length of the profile. This introduces an
436 additional parameter that is of influence for the damage: the position of
437 the irregularity (z_{SWL} , see figure 6). Research on a previous version of the
438 XblocPlus showed that the expected location of damage (initial extractions)
439 occurred between 1.0 and 1.5 H_s below the still waterline [Rada Mora, 2017].
440 Most effect of the irregularity could then reasonably be expected with the

441 irregularity placed around that depth. The irregularities were mostly placed
442 at a depth of $3.4 D_n$. Thus, for a typical stability number $H_s/(\Delta D_n)$ of 2.5,
443 the irregularity was placed at roughly $1 H_s$ under the water line, and for the
444 maximum stability number of 4.0, the top of the irregularity was placed at
445 $0.5 H_s$. Therefore the irregularity was placed around the location of high-
446 est wave attack, but possibly somewhat high for the tests with the largest
447 wave heights. The obtained test results confirm the influence of the depth
448 of the irregularity, since for example in series 5 of section 2 a higher placed
449 irregularity resulted in less damage.

450 As stated above, initial extractions of units typically occurred between
451 1.0 and $1.5 H_s$ below the water line [Rada Mora, 2017]. This damage location
452 around the rundown point of the waves is remarkable, as for typical rubble
453 mound (rock) slopes initial extraction often occurs around the water line,
454 where flow velocities are highest [De Almeida et al., 2019]. This location
455 could indicate that for this rather impermeable top layer, the damage is
456 (partly or largely) induced by excessive water pressures under the armour
457 layer during rundown of the wave, as occurs for placed-block revetments
458 [CUR, 1995].

459 The D_{n50} of both the core and underlayer are of the same size and grada-
460 tion. This choice has been made to prevent the thickness of the underlayer to
461 influence the results by introducing a variable permeability. Both the D_{n50}
462 and gradation have been chosen relatively small. The small element size
463 is expected to give a conservative result with respect to the stability [Bur-
464 charth and Andersen, 1995] and the grading is expected to have no significant
465 influence [Perrin et al., 2017].

466 The toe of the tested model was fixed and thus too stable in relation to
467 what would be designed in practice. At the locations where the armour layer
468 was located on a protruding (convex) irregularity under the mean water line
469 damage occurred during wave rundown. The armour layer at this location
470 was pushed outward by a combined effect of the weight of the upper armour
471 and the excessive hydraulic pressure of the remaining water under the armour
472 layer. This is less likely to occur with a toe structure that is barely sufficient.
473 Failure could then occur due to sliding of the toe, causing the breakwater
474 elements to slide along the slope as well. A lower crest of the structure may
475 result in the upper elements to be critical for damage, since the elements
476 gain stability by the weight of the elements above.

477 In this paper, the main slope was seen to be rather stable, and rela-
478 tively large irregularities seemed to be needed to significantly decrease the
479 stability of the blocks. However, in the tests a straight slope with a high non-
480 overtopped crest and with a fixed toe was considered. In realistic designs,
481 the origin of failure is often located at these outer edges of the slope (toe and
482 crest). Hence these items are a next item for further research. The toe could
483 slide away, when an entire Xbloc^{Plus} layer can place force on the toe, as was
484 observed for single layer cubes [Hofland and van Gent, 2016]. The upper rows
485 are not stabilized by the weight of rows on top of them, so for lower-crested
486 structures this might be the limiting factor for stability. The first application
487 of the Xbloc^{Plus} is the Afsluitdijk in the Netherlands, where 6.5 tonne units
488 are placed. Here the blocks are used on the lower slope. Hence the highest
489 element which is much less stable deserved extra attention [Janssen, 2018].

490 The Xbloc^{Plus} units resemble other recently developed units like cubes

491 that are placed in a single layer, the so-called C-ROC, and Seabees, as dis-
492 cussed in the introduction. These units can / are also placed in a regular
493 fashion, they obtain their stability mainly from friction, and they are placed
494 with such high density that pressures can build up underneath the layer.
495 Therefore it is likely that these units have a similar tolerance for uneven
496 placement as the presently studied unit. Hence when testing these types of
497 units a similar procedure with irregular placement of the under layer could
498 be followed. Moreover, the composition of the under layers is an important
499 characteristic of the design, as the pressures under the armour layer during
500 run down will be a function of the permeability of the under layer relative
501 to that of the amour layer. Conversely, damage mechanisms that have been
502 observed for other units (like the sliding of the toe due to the pressure of
503 a single layer of cubes), might well be expected to be an important failure
504 mechanism for the Xbloc^{Plus}.

505 The authors could not find much literature on the failure process of similar
506 single layer units. Most knowledge is developed in-house at licence holders,
507 and most findings seem to be reported in grey literature. Still we think it is
508 important that these failure mechanisms of similar units should be reported,
509 and based on the mechanisms that occur with other units. Hence, even
510 though this paper is based on tests on one type of unit, the authors believe
511 that the data and analyses presented might be relevant as it can serve as a
512 reference point for the studies on other types of units. The development of
513 the present units has been reported in various MSc theses at Delft University
514 of Technology (repository.tudelft.nl).

515 9. Conclusions

516 In total 177 test runs have been performed on a breakwater slope with an
517 armour consisting of regularly placed single layer interlocking units. Different
518 types of irregularities in the underlayer were applied, that could potentially
519 influence the interlocking of the elements. Based on these tests the following
520 conclusions have been drawn.

521 It is possible to measure the size of the underlayer irregularities and the
522 resulting orientation of breakwater elements by 3D reconstruction techniques
523 based on photogrammetry. Additionally the measurement technique was able
524 to indicate movements in the surface, which marks the initiation of damage.

525 Based on the results of the hydraulic model tests it can be concluded that
526 the level of stability for single layer breakwater elements decreases when the
527 size of the irregularities increases. An increase in the height of the irregu-
528 larities causes the relative angle between neighbouring elements to increase
529 which can lead to a loss of interlocking. Furthermore it increases the steep-
530 ness of the slope at the lower side of the irregularity, such that the under
531 layer becomes less resistant against being pushed outward.

532 The armour layer shows a maximum sensitivity to damage for convex de-
533 formations of the slope in the cross shore direction. A new failure mechanism
534 for initiation of damage, not previously observed for breakwater elements, has
535 been detected. This damage mechanism can occur when the armour layer
536 is located on a protruding (convex) irregularity under the mean water line.
537 During wave rundown the armour layer at this location is pushed outward
538 by a combined effect of the weight of the upper armour and the hydraulic
539 pressure of the remaining water under the top layer. The influence on the

540 stability is quantified well by a linear formula that depends on the relative
541 angle between the elements, caused by the radius of the irregularity, and the
542 steepness of the lower slope. The latter has only been seen to be of influ-
543 ence in the case of macro irregularities and thus seems to be insignificant for
544 micro irregularities. The steepness of the downward slope depends on both
545 the actual distance between the top of the irregularity and the design profile,
546 and the length scale of the irregularity.

547 The presently applied criteria for the placement of the underlayer for an
548 Xbloc^{Plus} breakwater element is a maximum deviation from the design profile
549 of 0.25 times D_n and a maximum deviation between succeeding measurements
550 of 0.10 times D_n . These deviations from the design slope are small compared
551 to the limiting value, such that the underlayer configuration will not influence
552 the stability significantly.

553 **References**

- 554 Angremond, K., Van Roode, F.C., Verhagen, H., 2008. Breakwaters and
555 closure dams. VSSD, Delft. 2nd edition.
- 556 Brouwer, M., 2013. The influence of the under layer on the stability of
557 single layer armour units Master of Science Thesis. Master thesis. Delft
558 University of Technology. Delft.
- 559 Burcharth, H., Andersen, O., 1995. On the One-Dimensional Unsteady
560 Porous Flow Equation. Coastal Engineering 24, 233–257.
- 561 CUR, 1995. Design manual for pitched slope protection. . Klein Breteler

562 for Ministry of Transport, Public Works and Water Management, Nether-
563 lands, Balkema, Rotterdam.

564 Dai, Y., Kamel, A., 1969. Scale effect tests for rubble-mound breakwaters:
565 Hydraulic model investigation. Technical Report H-69-2. U.S. Army En-
566 gineer Waterways Experiment Station. Washington D.C.

567 De Almeida, E., Gent, M.V., Hofland, B., 2019. Damage Characterization of
568 Rock Slopes. *J. of Marine Science and Eng* 7.

569 Docs.opencv.org, . OpenCV MatchTemplate documentation.

570 Garcia, N., Richardson, S., Rigden, T., 2013. Physical Model Testing of
571 the Hydraulic Stability of Single-layer Armour Units, in: *Coasts, Marine*
572 *Structures and Breakwaters Conference*, Institution of Civil Engineers, Ed-
573 inburgh.

574 Hofland, B., van Gent, M., 2016. Automatic settlement analysis of single-
575 layer armour layers, in: *International Conference on the Application of*
576 *Physical Modelling in Coastal and Port Engineering and Science*, Coastlab,
577 Ottawa.

578 Hudson, R.Y., 1959. Laboratory investigation of rubble-mound breakwaters.
579 Technical Report. American Society of Civil Engineers. Vicksburg.

580 Jacobs, R., 2017. Internal memo; 2D Hydraulic Model Tests. Technical
581 Report. Delta Marine Consultants. Gouda.

582 Janssen, D., 2018. Stability analysis of XblocPlus crest element. Master
583 thesis. Delft University of Technology.

- 584 Loman, G., Hofland, B., van der Biezen, S., Poot, J., 2012. Integral design of
585 hard sea defense of Maasvlakte 2, Part II: Physical model testing of cube
586 revetment and reef, in: Coastlab12, Ghent University, Ghent.
- 587 Van der Meer, J., 1988. Stability of Cubes, Tetrapods and Accropode, in:
588 Conference Breakwaters '88, Delft Hydraulics Laboratory, London. pp. 59–
589 68.
- 590 ten Oever, E., Verhagen, H.J., Klabbers, M., Reedijk, B., 2012. Theoretical
591 and experimental study on the placement of Xbloc armour units, in: In-
592 ternational Conference on Coastal Engineering, American Society of Civil
593 Engineers, San Diego.
- 594 Pardo, V., Herrera, M.P., Molines, J., Medina, J.R., 2013. Placement grids,
595 porosity and randomness of armor layers. *Waterway, Port, Coastal, and*
596 *Ocean Engineering* 140.
- 597 Perrin, S., Giraudel, C., Collinsworth, S., Melby, J., 2017. Hydraulic response
598 & placement methods for a new single-layer concrete armour unit called
599 C- ROC TM, in: *Coasts, Marine Structures and Breakwaters Conference*,
600 *Institution of Civil Engineers, Liverpool*.
- 601 Rada Mora, B., 2017. Hydraulic performance of Xbloc+ armor unit. Master
602 thesis. Delft University of Technology.
- 603 Van Gent, M., Luis, L., 2013. Application of cubes in a single layer, in: *Inter-*
604 *national Short Course/Conference on Applied Coastal Research, SCACR*.
- 605 Vos, A.B., 2017. Exploration into the mechanisms that govern the stability of
606 an Xbloc+ v1 armour unit. Master thesis. Delft University of Technology.

607 Van der Zicht, B., 2015. Specifications of Application Xbloc. Technical
608 Report. Delta Marine Consultants. Gouda.